

Near-shore talik development beneath shallow water in expanding thermokarst lakes, Old Crow Flats, Yukon

Pascale Roy-Leveillee,^{1, 2} and Christopher R. Burn,²

Corresponding author: Pascale Roy-Leveillee, School of Northern and Community Studies, Laurentian University, 935 Ramsey lake Road, Sudbury, ON, P3E 2C6, Canada.
(proyleveillee@laurentian.ca)

¹School of Northern and Community Studies, Laurentian University, Sudbury, ON, Canada.

²Department of Geography and Environmental Studies, Carleton University, Ottawa, ON, Canada.

This article has been accepted for publication and undergone full peer review but has not been through the copyediting, typesetting, pagination and proofreading process, which may lead to differences between this version and the Version of Record. Please cite this article as doi: 10.1002/2016JF004022

Abstract.

It is generally assumed that permafrost is preserved beneath shallow lakes and ponds in the Western North American Arctic where water depth is less than about 2/3 of the late-winter lake-ice thickness. Here, we present field observations of talik development beneath water as shallow as 0.2 m despite a lake-ice thickness of 1.5 m, in Old Crow Flats (OCF), YT. Conditions leading to the initiation and development of taliks beneath shallow water were investigated with field measurements of shore erosion rates, bathymetry, ice thickness, snow accumulation, and lake-bottom temperature near the shores of two expanding lakes in OCF. The sensitivity of talik development to variations in lake-bottom thermal regime was then investigated numerically. Where ice reached the lake bottom, talik development was controlled by the ratio of freezing degree-days to thawing degree-days at the lake bottom (FDD_{lb}/TDD_{lb}). In some cases, spatial variations in on-ice snow depth had a minimal effect on annual mean lake-bottom temperature (T_{lb}) but caused sufficient variations in FDD_{lb}/TDD_{lb} to influence talik development. Where T_{lb} was close to but greater than 0°C simulations indicated that the thermal offset allowed permafrost aggradation to occur under certain conditions, resulting in irregular near-shore talik geometries. The results highlight the sensitivity of permafrost to small changes in lake-bottom thermal conditions where the water column freezes through in early winter and indicate the occurrence of permafrost degradation beneath very shallow water in the near-shore zone of Arctic ponds and lakes.

1. Introduction

Thermokarst lakes are widespread in circumpolar regions and a significant source of atmospheric methane, as the unfrozen ground, or talik, that develops beneath them provides an anaerobic environment wherein bacteria decompose organic matter formerly preserved in permafrost [Walter *et al.*, 2006; Olefeldt *et al.*, 2016]. Methane release from taliks is most active at the thaw front and is concentrated near receding lake margins [Walter *et al.*, 2006; Kessler *et al.*, 2012]. Talik development near the edge of lakes is thus important for predictions of methane flux from thermokarst lowlands, particularly as a warming climate may cause permafrost to degrade beneath shallow water, where it was previously sustained [Burn, 2002; Arp *et al.*, 2016]. Nevertheless, field observations of talik geometry near thermokarst shorelines [e.g., Burn and Smith, 1990; Burn, 2002; Schwamborn *et al.*, 2002] are scarce and it is commonly assumed, from data collected in the Mackenzie delta area by Mackay [1992], that permafrost is sustained under water depths less than two thirds of the late-winter ice thickness [e.g., Rowland *et al.*, 2011; Matell *et al.*, 2013; Arp *et al.*, 2016]. The general practice when modelling talik development is to use annual mean lake-bottom temperature (T_b) to represent lake-bottom thermal conditions, and assume that variations in lake-bottom thermal regime which affect talik development are captured by this value [e.g., West and Plug, 2008; Matell *et al.*, 2013].

In this study, we present field observations of taliks beneath very shallow water near the shores of expanding thermokarst lakes in Old Crow Flats (OCF), northern Yukon (Fig. 1). We use a numerical model to investigate controls on talik initiation and development in this environment, with a focus on sensitivity to aspects of the lake-bottom thermal

regime which may not be reflected in the annual mean lake-bottom temperature (T_{lb}). In particular, we examine the ratio of freezing degree days (FDD_{lb}) to thawing degree days (TDD_{lb}) at the lake bottom. FDD_{lb} and TDD_{lb} are the cumulative departures from 0°C in mean daily temperatures ($^{\circ}\text{C d}$) during the freezing and thawing seasons, respectively.

In permafrost regions, surface water causes the greatest local departures of ground temperatures from geographical patterns determined by climate [*Lachenbruch et al.*, 1962]. Ground beneath lakes is warmer than the surrounding permafrost because lake-bottom temperature remains $\geq 0^{\circ}\text{C}$ until the ice contacts the lake bottom. As a result, permafrost cannot be sustained proximally to the lake bottom beneath water that is deeper than the thickness of lake ice [*Mackay*, 1963]. Under such conditions, predictive models based on mean annual temperatures, such as the Stefan solution, have been used successfully to predict talik development beneath expanding Arctic and subarctic thermokarst lakes [e.g., *Burn and Smith*, 1990; *Burn*, 2002]. Several numerical solutions based on mean annual temperatures have been used to calculate transient ground temperatures near shifting water-land boundaries [e.g., *Hwang and Smith*, 1973; *Ling and Zhang*, 2003; *West and Plug*, 2008]. These models consider cases where water depth exceeds the mean maximum ice thickness. Yet shallow lakes, with water depths \leq the regional long-term maximum ice thickness, are abundant throughout the Arctic [*Duguay and Lafleur*, 2003; *Arp et al.*, 2011; *Morgenstern et al.*, 2011].

Where water depth \leq lake-ice thickness, a talik develops if thaw penetration exceeds the depth of seasonal frost penetration, or active layer, in the lake-bottom sediment [*Mackay*, 1992]. Few models consider talik development under such conditions, as available field data suggest that T_{lb} are $\leq 0^{\circ}\text{C}$ [*Brewer*, 1958; *Burn*, 2005; *Arp et al.*, 2016] and that

permafrost is sustained beneath shallow water that freezes to the lake bottom in early winter [Mackay, 1992; Burn, 2002; Schwamborn et al., 2002; Stevens et al., 2010]. In this study we describe observations of talik development beneath shallow, relatively flat-bottomed, tundra lakes that freeze to the bottom over extended areas.

Where thermal conditions at the ground surface are close to, but above 0°C, permafrost sustainability is controlled by the thermal offset, which is the difference between annual mean temperature at the ground surface, in this case T_{lb} , and annual mean temperature at the top of permafrost [Kudryavtsev, 1981; Burn and Smith, 1988; Romanovsky and Osterkamp, 1995]. The thermal offset results from the difference in temperatures required to achieve an equilibrium annual heat balance of 0 W with differing thermal conductivities for frozen (λ_f) and thawed ground (λ_t). The limit of permafrost sustainability, where mean temperature at the bottom of the seasonally frozen layer is 0°C, occurs where the ratio of freezing to thawing degree days at the lake bottom, FDD_{lb}/TDD_{lb} , is equal to λ_t/λ_f [Romanovsky and Osterkamp, 1995; Smith and Riseborough, 1996].

At the lake bottom, the freezing season extends through the duration of ice contact with the lake bottom. FDD_{lb} generally increase with the duration of ice contact with the lake bottom, and decrease with increasing water depths, winter air temperatures, and on-ice snow thickness. TDD_{lb} generally increase with decreasing water depth and with increasing summer air temperatures, mixing, and depth of solar radiation penetration. In the saturated lake bottom sediment, λ_t/λ_f is controlled by the material moisture content and the difference in thermal conductivity between ice and water. In the case of fine-grained deposits, such as glaciolacustrine silts and clays, the unfrozen water content of the cryotic sediment reduces the effective λ_f which, in reality, is not a single value

but a function of sediment temperature below 0°C [*Romanovsky and Osterkamp, 2000; Riseborough, 2002*]. This results in increased permafrost vulnerability as it shifts the limit of permafrost sustainability towards higher FDD_{lb}/TDD_{lb} . Permafrost sustainability beneath the bottom-fast ice of the outer Mackenzie Delta was effectively assessed by *Stevens et al.* [2010] based on these principles.

This study aims to improve understanding of talik development near the shorelines of shallow thermokarst lakes by using field observations from a tundra area of OCF (Fig. 1b) and numerical modelling to examine aspects of the lake-bottom thermal regime that control permafrost degradation beneath shallow water and near thermokarst lake shores.

The specific objectives of this research are to: (1) measure lake-bottom temperatures near shorelines of thermokarst lakes in OCF; (2) delineate and compare talik geometry near shorelines with varying erosion rates, bathymetries, and lake-bottom thermal regimes; and (3) assess the sensitivity of permafrost degradation rates beneath shallow water near these shorelines to variations in FDD_{lb}/TDD_{lb} using a numerical model of ground freezing and thawing.

2. Study Area: The Old Crow Flats

OCF is a 5600 km² lowland in Old Crow basin, northern Yukon, that was not glaciated during the Wisconsinan period, but was submerged beneath Glacial Lake Old Crow (Fig. 1a). The lake deposited up to 9 m of unfossiliferous glaciolacustrine sediment over thick layered Pleistocene sands and silts [*Lichti-Federovich, 1973; Duk-Rodkin et al., 2004*]. Glacial Lake Old Crow persisted until 14.8 ka BP [*Zazula et al., 2004*] and permafrost developed in the freshly exposed sediments following catastrophic drainage of the glacial lake [*Lauriol et al., 2009*]. River-bank exposures suggest that the glaciolacustrine sedi-

ments are the sole stratigraphic layer with excess ground ice in the upper 40 m of deposits [Matthews *et al.*, 1990]. The only regional data on permafrost thickness are from the community of Old Crow, where the base of permafrost is 63 m below the ground surface [EBA Engineering Consultants Ltd, 1982].

Lakes cover approximately 35% of OCF [Yukon Ecoregions Working Group, 2004] (Fig. 1b). Some of these may be remnants of Glacial Lake Old Crow [Ovenden, 1985], but many likely developed by thermokarst processes during the early Holocene thermal optimum [Mackay, 1992; Burn, 1997], when July temperatures in OCF were approximately 6°C higher than at present [Lauriol *et al.*, 2002]. The lakes lack littoral shelves, and are generally flat-bottomed and shallow, with a mean depth of about 1.5 m [Gray and Alt, 2001]. The bathymetry reflects the limited thickness of ground ice in the Flats. However, lake expansion by thermokarst processes is apparent throughout OCF, indicating that near-surface ground ice is common [Roy-Leveillee and Burn, 2015]. There are many drained lake basins with incised outlets, suggesting that catastrophic drainage is part of the natural evolution of many lakes [Lantz and Turner, 2015; Roy-Leveillee and Burn, 2016]. Dates from basal peat samples collected in OCF suggest that much of the area has been reworked by thermokarst processes over the last 10,000 years [Ovenden, 1985].

In 1981-2010, the mean annual air temperature at Old Crow was -8.3°C, with mean monthly air temperatures ranging from 14.6°C (July) to -29.2°C (January) (Environment Canada climate data are available at <http://climate.weather.gc.ca/>, accessed on April 26st, 2016). Average annual total precipitation was 279 mm, with 55% of the precipitation arriving as rain. During 2008-11, the annual mean air temperature, calculated as the average of daily mean temperatures between September 1st and August 31st, varied between

-9.4 and -6.5°C (Table 1). The warmest year was 2009-10, due to high temperatures from February to May, and the coldest was 2008-09, due to low temperatures in fall and winter. Summer air temperatures were similar each year. Precipitation was higher than normal in 2010-11, particularly in February (155 mm) and June (162 mm).

The study area for this research is in the tundra portion of OCF, where lakes and drained lake basins commonly have rectilinear shorelines oriented NE-SW or NW-SE (Fig. 1) [Roy-Leveillee and Burn, 2015, 2016]. The lakes are surrounded by extensive networks of ice-wedge polygons. *Sphagnum* spp. mosses, cotton-grass (*Eriophorum* spp.) tussocks, salmonberry (*Rubus chamaemorus*) and dwarf birch (*Betula glandulosa*) generally cover the polygon centres, while ericaceous shrubs, willows (*Salix* spp.) and alders (*Alnus* spp.) grow on the dryer ridges at the rims of the polygons. *Salix* and *Alnus* bushes up to 3 m high are also found along some of the lake shores, where the banks are higher than 1 m and low erosion rates permit vegetation development. Permafrost temperatures in the study area vary interannually with snowfall and air temperature and spatially with the snow holding capacity of the vegetation cover. Near the depth of zero annual amplitude, more than 14 m below the surface, mean ground temperatures measured in 2009-2013 were -5.1°C in low shrub (≤ 0.6 m high) polygonal tundra and -4.6°C where tall shrubs (≥ 1 m high) grow on ice-wedge ridges [Roy-Léveillé et al., 2014]. Peat thickness in OCF varies between 0.3 and 1.0 m and the dates on basal peat samples range from approximately 350 to 3300 ^{14}C a BP [Ovenden, 1985]. Basal peat collected at 0.8 m depth in the study area was dated at 2215 ± 93 cal BP (UCIAMS # 67161) [Roy-Leveillee and Burn, 2016].

3. Methods

3.1. Field methods

The first two objectives of this study included the measurement of lake-bottom temperatures and the delineations of talik geometry near thermokarst lakeshores with varying erosion rates, bathymetries, and lake-bottom thermal regimes. In 2008, four study sites were selected for this purpose on adjacent lakes representing a range of shoreline conditions (Fig. 1; Table 2). The study sites comprise a lake-bottom transect and nearby ground monitoring installations. The ice-wedge polygons at sites 1 and 2 were in low-shrub tundra whereas tall shrubs characterized sites 3 and 4. At the latter sites, shrub abundance increased at the bank top, and shrubby vegetation extended to the waterline (Fig. 2).

In spring of 2009 and 2010, lake ice was used as a drilling platform to delineate the base of the sub-lake talik along four lines perpendicular to shore, one at each site. Holes were augered in the ice at 10-m intervals to measure lake depths. Frozen ground at the bottom of the talik was detected in the same holes by sudden resistance to penetration of a water-jet drill [Burn and Smith, 1990]. Near-shore lake-bottom temperatures were monitored and recorded every four hours from August 2008 to August 2011 by Onset HOBO H8 data loggers (range of internal temperature sensor: -40°C to 100°C , accuracy: $\pm 0.7^{\circ}\text{C}$ and resolution: $\pm 0.4^{\circ}\text{C}$ at 0°C) placed in waterproof capsules that were attached to the shore with steel line and anchored to the lake bottom (Fig. 1). In late winter 2009 and 2010, snow depth and ice thickness were measured at each data-logger location, and in several locations near the centre of the lakes, where ice did not reach the lake bottom, to assess maximum lake-ice thickness. Temperature near the permafrost surface was recorded from August 2008 to August 2011 in undisturbed ground within 50 m of the lake shore (Fig. 1). Temperature sensors (Onset Corp. TMC6-HA, range: -40°C to

100°C, accuracy: $\pm 0.5^\circ\text{C}$ and resolution: $\pm 0.4^\circ\text{C}$ at 0°C) were installed 1.25 m below the ground surface and connected to HOBO H8 data loggers to record ground temperature every 4 hours. A HOBO H8 data logger and TMC6-HA temperature sensor were also used to measure air temperature 1.5 m above the ground in a radiation shelter between sites 1 and 4 from August 2009 to September 2011.

3.2. Ground material properties

Sets of permafrost core samples were extracted with a Cold Regions Research and Engineering Laboratory (CRREL) drill to assess properties of the ground material in the area. Two sets of permafrost core samples extending to a depth of 1.5 m below the ground surface were extracted from the bank top near each site. During late winter 2010, two additional sets of samples were extracted from the lake bottom near the foot of a rapidly receding shore bank at Site 1. The upper sections of the latter two sets were examined to identify and eliminate bank debris and reworked lake sediment based on organic contents and breaks in cryostratigraphic structure, and to keep parts of the samples representing permafrost that had not yet thawed.

Core sections were thawed, mixed, poured into beakers, weighed, and allowed to settle according to a method suitable for silt loams [Kokelj and Burn, 2003]. Volumes of saturated sediment (V_{ss}) and supernatant water (V_{sw}) were recorded to provide a conservative estimate of the volumetric excess ice content (V_i %) of the samples using eq. 1 [Kokelj and Burn, 2003]:

$$V_i = \left[\frac{1.09V_{sw}}{V_{ss} + (1.09V_{sw})} \right] 100 \quad (1)$$

Total water contents were determined by oven drying the sediments at 105°C, and V_{sw} was subtracted from the total water content to estimate porosity (p). Organic contents of the cores were estimated by loss on ignition at 550°C and sediment textures of these cores were determined by the pipette method [Sheldrick, 1984].

Thermal properties of the ground material were based on lake-bottom core samples (Tables 3, 4). The thawing characteristic curve was a function typical for silt loam, the grain size of the soil found at the study sites, where the gravimetric unfrozen water content (w_u , g g⁻¹) was calculated for various temperature (t) below 0°C using parameters presented by *Andersland and Ladanyi* [2003, Table 2.6] based on *Smith and Tice* [1988, Appendix A] (eq. 2):

$$w_u = 6.0 | T |^{-0.301} \quad (2)$$

The thermal conductivities (λ) of thawed and frozen sediments were calculated based on this thawing characteristic curve using a geometric mean (eq. 3). The water and ice fractions were determined using the unfrozen water content characteristic curve to determine the proportion of soil pore water that is unfrozen ($u\%$) [Johansen, 1975].

$$\lambda = (\lambda_w^{u\%p}) (\lambda_i^{V_i+(1-u\%)p}) (\lambda_o^{V_o}) (\lambda_m^{1-p-V_i-V_o}) \quad (3)$$

Thermal conductivities of 0.56, 2.24, 0.25, and 2.92 W m⁻¹ °C⁻¹ were used for the water (λ_w), ice (λ_i), organic (λ_o), and mineral (λ_m) components, respectively [Williams and Smith, 1989]. The volumetric organic and mineral contents (V_o ; V_m) were estimated using the average organic gravimetric fraction (O_g) obtained from loss on ignition, and assuming densities of 1.30 x 10⁶ g m⁻³ for organic matter and 2.65 x 10⁶ g m⁻³ for the mineral fraction [Williams and Smith, 1989]. The volumetric heat capacities (C) of thawed and

frozen sediment were calculated using a weighted arithmetic mean (eq. 4) where values of 4180, 1296, 2385, 2496 kJ m⁻³ °C⁻¹ were used for the volumetric capacities of water (C_w), ice (C_i), mineral (C_m), and dry organic components (C_o), respectively [Williams and Smith, 1989].

$$C = [C_w p u\% + C_i (V_i + (1 - u\%)p) + C_o V_o + C_m (1 - p - V_i - V_o)] \quad (4)$$

3.3. Determination of shore erosion rates

Shore-bank recession rates were measured to assess time since submergence for parts of the lake bottom at different distances from the shore. Erosion rates were monitored using benchmarks installed near each study line during the 2009, 2010, and 2011 open-water seasons. Calculated uncertainty in short-term erosion rates was determined on a site-by-site basis based on the precision of measurements. The latter depended on the abruptness of the break in slope marking the top of the bank, and ranged from 0.05 to 0.4 m. Rates of shore erosion measured in the field were compared to long-term erosion rates determined from aerial photographs of the study sites taken in 1951 and 1996. The scanned photographs were superimposed using ice-wedge networks near the four sites to co-register the images. Uncertainty in shoreline location was assessed based on picture quality and resolution and ranged from 0.6 to 1.9 m.

3.4. Numerical simulations

Models that use mean annual temperatures to define surface conditions do not include characteristics of the thermal regime such as the duration of freezing and thawing at the lake bottom. The third objective of this research was to assess the sensitivity of permafrost degradation rates beneath shallow water near shorelines to variations in

FDD_{lb}/TDD_{lb} using a numerical model of ground freezing and thawing. Three numerical simulations investigated how variation in the lake-bottom thermal regime, particularly in FDD_{lb}/TDD_{lb} , may affect talik initiation, development rate, and refreezing under conditions similar to the study sites.

Thaw front penetration in the lake-bottom sediment was modelled with Temp/W (Release 7.03, GEO-SLOPE International Ltd.), a commercially available package that calculates finite element numerical solutions for conductive heat-transfer problems. It accounts for temperature-dependent thermal properties such as volumetric unfrozen water content (θ , $\text{m}^3 \text{ m}^{-3}$) and latent heat effects associated with phase change through an apparent heat capacity (C_a , $\text{J m}^{-3} \text{ }^\circ\text{C}^{-1}$) (eq. 5):

$$C_a = C + L \frac{\partial \theta_u}{\partial T} \quad (5)$$

Eq. 6, where Q is the applied boundary heat flux (W m^{-1}), is the governing differential equation for the model [*GEO-SLOPE International Ltd*, 2010]:

$$\frac{\partial}{\partial x} \left(\lambda_x \frac{\partial T}{\partial x} \right) + \frac{\partial}{\partial y} \left(\lambda_y \frac{\partial T}{\partial y} \right) + Q = C_a \frac{\partial T}{\partial t} \quad (6)$$

Temp/W has been used in several permafrost studies [e.g., *Stevens et al.*, 2010; *Kokelj et al.*, 2014] including studies of talik development beneath lakes in the Mackenzie Delta region at time scales varying from decades to several thousand years [*Taylor et al.*, 2008; *Kokelj et al.*, 2009].

Thaw front penetration and thermal conditions beneath the lake bottom were simulated in one dimension, over a depth of 100 m. The simulation domain was discretized with a vertical spacing of 0.01 m in the upper metre, 0.05 m to a depth of 5 m, 0.1 m to a depth of 10 m, 0.5 m to a depth of 50 m, and 1 m to a depth of 100 m. A geothermal heat flux

of 0.07 W/m^2 was used as the lower boundary condition [Blackwell and Richards, 2004].

The upper boundary represented thermal conditions near the ground surface either at the top of permafrost, when simulating subaerial conditions prior to submergence, or at the lake bottom, when simulating talik development after submergence.

Simulated conditions prior to submergence and talik development were based on the estimated duration of subaerial exposure at the study area inferred from a basal peat date of 2215 ± 93 cal BP (UCIAMS # 67161) [Roy-Leveillee and Burn, 2016] collected near Site 2 and on measurements of temperature at the top of permafrost (T_{ps}) as described above. Steady-state equilibrium conditions with $T_{lb} = 4.5 \text{ }^\circ\text{C}$, as under a large lake, were followed by 2000 years of subaerial conditions with a T_{ps} of $-4.0 \text{ }^\circ\text{C}$, based on the average (T_{ps}) measured near sites 2, 3, and 4. Simulations of talik development began from that point. Unless otherwise specified, daily time steps were used with daily mean lake-bottom temperatures as the upper boundary condition. Progress of the thawing or freezing front was extracted every year during late spring when mean daily lake-bottom temperature first reached 0°C , to assess whether a talik began to develop or how far it extended below the lake bottom. The talik boundary was defined as the -0.005°C isotherm, to avoid including ground that was isothermal at or slightly below 0°C . Where ground cooling and refreezing occurred, this ensured that the talik boundary was located at the limit of the zone where freezing had really begun rather than at the top of the zero curtain, and had very little influence on talik depth in simulations which did not involve talik refreezing.

Empirical data collected at the study sites were used to drive the simulations to ensure that the conditions tested were realistic and directly relevant to observed conditions at the study sites. Measured lake-bottom temperatures were used to define upper-boundary

conditions, rather than a surface energy balance at the water and on-ice snow cover surfaces, to keep the model simple and focus on the sensitivity of talik development to changes in the lake-bottom thermal regime.

3.4.1. Talik initiation and the occurrence of years with warm conditions

As climatic warming continues, years with warmer than normal lake-bottom conditions may occur more frequently [Arp *et al.*, 2016]. A first numerical simulation examined the effect on talik initiation and establishment beneath shallow water of occasional years with warm lake-bottom conditions. Upper-boundary conditions were defined with mean daily temperatures recorded at Site 2, 16 m from the shore. Temperatures recorded in 2009-10 ($T_{lb} = 1.9^{\circ}\text{C}$, $FDD/TDD = 0.51 \approx \lambda_t/\lambda_f$, see Table 3), expected to be just sufficiently warm for permafrost degradation, were cycled at the surface. Annual records from 2010-11 ($T_{lb} = 3.3^{\circ}\text{C}$, $FDD/TDD = 0.18$), when lake-bottom conditions were substantially warmer, were inserted at regular intervals. Four thermal environments were simulated to examine the effects of increasing warm year occurrences on conditions that are marginal for talik initiation: (1) 2009-10 data alone as a base case; (2) 2010-11 inserted every third year; (3) 2010-11 inserted every second year; and (4) 2010-11 data alone.

3.4.2. Talik development rate and FDD_{lb}/TDD_{lb}

Predicted regional increases in summer temperature and snow accumulation [Maloney *et al.*, 2013; Bintanja and Selten, 2014] could result in a decrease in the ratio of freezing to thawing degree days (FDD_{lb}/TDD_{lb}) at the lake bottom where the water column freezes through. Variation in FDD_{lb}/TDD_{lb} associated with changes in the amplitude of the annual thermal regime at the lake bottom may not be captured by T_{lb} , so a second numerical simulation of near-shore talik development examined the effects of varying FDD_{lb}/TDD_{lb}

ratios while keeping T_{lb} constant. Upper boundary conditions were defined using lake-bottom thermal regimes with FDD_{lb}/TDD_{lb} varying from 0.01 to 0.65 to represent a range of field conditions (Fig. 3). All the lake-bottom thermal regimes applied had a T_{lb} of 2.00°C and 252 days of ice contact with the lake bottom, to insure assessment of sensitivity to variations in FDD_{lb}/TDD_{lb} specifically. Such variations in FDD_{lb}/TDD_{lb} beneath shallow water could result from changes in summer or winter air temperatures, in water levels, or in the on-ice snow cover during ice contact with the lake bottom. The simulations were conducted over 100 years.

3.4.3. Talik refreezing with T_{lb} above 0°C

Talik refreezing may occur near receding shores where water is shallow and frost penetrates the lake bottom. It is commonly assumed that taliks develop where $T_{lb} > 0^{\circ}\text{C}$ and that permafrost aggradation is limited to conditions with $T_{lb} < 0^{\circ}\text{C}$. However, where T_{lb} is close to but greater than 0°C permafrost sustainability is controlled by the thermal offset [Smith and Riseborough, 2002]. A third numerical simulation investigated whether talik refreezing may occur under thermal conditions observed in OCF during our study, when T_{lb} was $> 0^{\circ}\text{C}$. To assess this, the development of a talik 6.5 m deep was simulated by applying a T_{lb} of 2.4°C for 60 years after spin-up, and talik development was examined over the following 100 years using six different upper boundary conditions representing a range of thermal regimes with $T_{lb} > 0^{\circ}\text{C}$ and FDD_{lb}/TDD_{lb} varying from 0.37 to 0.65. Five of these conditions used mean daily lake-bottom temperatures and one was based on an annual mean lake-bottom temperature. These upper boundary conditions were defined with mean daily temperatures recorded (1) 6 m from shore at Site 2 in 2009-10 ($T_{lb} = 1.5^{\circ}\text{C}$, $FDD_{lb}/TDD_{lb} = 0.60$); (2) 16 m from shore at Site 2 in

2009-10 ($T_{lb} = 1.9^{\circ}\text{C}$, $FDD_{lb}/TDD_{lb} = 0.51$); (3) 20 m from shore at Site 3 in 2009-10 ($T_{lb} = 1.4^{\circ}\text{C}$, $FDD_{lb}/TDD_{lb} = 0.65$); (4) 15 m from shore at Site 4 in 2010-11 ($T_{lb} = 2.4^{\circ}\text{C}$, $FDD_{lb}/TDD_{lb} = 0.37$); (5) 35 m from shore at Site 4 in 2010-11 ($T_{lb} = 2.2^{\circ}\text{C}$, $FDD_{lb}/TDD_{lb} = 0.44$); and (6) the annual mean lake-bottom temperature recorded 20 m from shore at Site 3 in 2009-10 ($T_{lb} = 1.4^{\circ}\text{C}$, $FDD_{lb}/TDD_{lb} = 0$).

4. Results

4.1. Field results

This study examined aspects of the lake-bottom thermal regime that control permafrost degradation beneath shallow water near thermokarst lakeshores. In this section we present field observations of near-shore lake-bottom thermal regimes and talik geometry from four sites representing a range of conditions in a tundra area of OCF (Fig. 1b).

4.1.1. Permafrost conditions

Annual mean temperatures near the top of permafrost were approximately 1°C lower in the low shrubs near Site 2 than in the tall shrubs of sites 3 and 4 (Table 5). Estimates of volumetric segregated and pore-ice content (I_c) in the top metre of permafrost ranged between 14% and 31% with a mean of 22%. A layer of ice-rich ground was observed approximately 1 m below the surface at all sites. Well-developed ice wedge networks were present near the four sites, and extended to depths of 2 to 3 m in the bank exposure near Site 1. Analysis of the core samples extracted from the foot of the rapidly receding bank near Site 1 indicated that segregated ice content was reduced below 3 m depth (Table 4). The average moisture content in the lake-bottom samples was 49%. The samples were silt loams with a sandy layer near 1.5 m below the lake bottom and the mean sand, silt

and clay volumetric fractions of the mineral sediment were respectively 20, 67, and 13%.

The average gravimetric organic content of the dry soil was estimated at 6%.

4.1.2. Lake ice and snow cover

The thickness of floating ice varied between 1.04 and 1.55 m in late winter, with a mean of 1.30 m (n=7) in 2009 and 1.45 m (n=3) in 2010. At temperature monitoring sites where water depth was less than the late-winter ice thickness, ice contact with the sediment generally occurred in October or November (Table 6).

The thickest on-ice snow drifts occurred at sites 1 and 4 (Fig. 4). These sites had high shore banks facing NE and SW, respectively, which correspond to the dominant wind directions in the area [*Yukon Ecoregions Working Group, 2004*] and, in the case of Site 4, tall shrubs near the edge of the lake. These conditions resulted in snow drifts over 2 m thick that extended 45 m from shore at Site 1 and 30 m from shore at Site 4. In contrast at Site 2, where the shore bank was 1 m high and the bank top vegetation was low shrub tundra, the snow drift was 0.73 m thick and extended less than 10 m onto the lake from the bank. Site 3 had a high bank with a well developed cover of tall shrubs but a less favourable orientation for snow accumulation, and the 1.2-m thick snow drift ended less than 10 m from the shore (Fig. 4).

4.1.3. Bathymetry

The two lakes were relatively flat-bottomed and shallow, like the majority of lakes in OCF. The reported mean lake depth of 1.5 m [*Gray and Alt, 2001*] is slightly less than the maximum ice thickness measured in this study and suggests that water in a significant portion of the lakes may freeze to the bottom. Both lakes included shoreline sections

where near-shore water was shallow, such as at Site 4, and areas where near-shore water was relatively deep, such as sites 1 and 2.

Lake depth along the surveyed transects rarely exceeded 2.5 m. A maximum depth of 3.1 m was measured 200 m from shore near Site 1, while on the smaller lake the maximum water depth measured was 2.3 m, 40 m from shore at Site 2 (Fig. 4). The lake-bottom sloped gently away from the shoreline until a lake depth of approximately 2 m was reached. At sites 1 and 2, this slope extended approximately 40 m from the shore (Fig. 4). At Site 4, the mean lake depth was reached more than 200 m from the shore, and lake depth was less than 1.5 m up to 130 m from the bank.

4.1.4. Lake-bottom temperatures

Annual mean lake-bottom temperatures (T_{lb}) were $>0^{\circ}\text{C}$ at all measurement sites. T_{lb} were between 4 and 5°C at a site where water depth was close to the maximum ice thickness and contact between the ice cover and bottom sediment occurred in March (Fig. 5a, Table 6). T_{lb} varied between 1 and 2°C at the other sites, beneath shallow water, in most years. Higher T_{lb} were recorded in 2010-11, a year with reduced FDD_{lb} in early winter and increased snowfall (Table 1).

A snow drift developed over the near-shore shallow water area at sites 1, 3 and 4 (Fig. 4). At sites 3 and 4, where lake-bottom temperatures were monitored beneath the snow drift and further from shore, FDD_{lb} near the lake edge were lower than or equal to FDD_{lb} further from the bank beneath deeper water. At Site 4 in 2010-11, there were 103 less FDD_{lb} beneath the near-shore snow drift than below a thin snow cover, even though the ice reached the lake bottom earlier near shore (Fig. 5b). At Site 3, there were 50 less FDD_{lb} beneath the near shore snow drift than further away from shore beneath a thin

snow cover in 2008-09, and 26 less FDD_{lb} in 2009-10, despite a 0.4 m difference in water depth and earlier ice contact with the lake bottom near shore. The opposite relation was observed at this site in 2010-11, with 527 more FDD_{lb} near shore (789 vs 262), possibly due to high overall snow depth reducing heat loss beyond the usual extent of the snow drift.

4.1.5. Frost penetration in the lake bottom

A superficial layer of frozen sediment was encountered at all sites where ice was in contact with the lake bottom in May 2009. This seasonally frozen sediment extended 15, 20, 43, and 150 m from shore at sites 1, 2, 3 and 4 respectively, and had a maximum thickness of 2.40 m, 4 m from shore at Site 4. Active layer freeze-back was only observed for a short distance from shore at sites 1, 2, and 3 (Table 7). It was observed furthest from shore at Site 2, where the snow drift was thinnest and frost penetration deepest (Table 7). These data indicate that permafrost may be sustained more extensively beneath shallow water near shore if the on-ice snow depth declines, as observed by *Stevens et al.* [2010] in the outer Mackenzie Delta.

4.1.6. Shoreline erosion

Erosion rates ranged from 0.13 ± 0.06 to 2.00 ± 0.07 m a⁻¹ between 1951 and 1996, whereas erosion rates measured in the field between 2009 and 2011 ranged from 0 ± 0.3 to 3.9 ± 0.1 m a⁻¹ (Table 8). The two shorelines with a NE aspect, sites 1 and 2, showed the highest erosion rates, had more exposed soil, occasionally developed overhanging peat curtains and erosional niches, and had deeper water near shore (Fig. 2, Table 2). At Site 4, with an extended zone of shallow water near shore, there was little shoreline erosion (Table 8).

4.1.7. Talik geometry

The talik began near the edge of the lake at all four sites (Table 7). The basal slopes of the taliks were lowest at sites 1 and 2 where shore erosion was most rapid (Fig. 6). Talik slopes followed a relatively uniform linear or concave shape at sites 1, 2 and 3. A break in slope near shore, where lake water froze to the bottom early in winter, formed a small near-shore shelf at the base of the talik at sites 1, 2, and 3 (Fig. 6, indicated by arrows). The feature was difficult to distinguish at Site 2. An extended shelf was observed in the talik boundary at Site 4, where water was shallow and the ice reached the lake bottom for a long distance from the shore. A 2.4-m deep depression occurred in this shelf under the area of the near-shore snow drift (Fig. 6).

4.2. Modelling results

4.2.1. Talik initiation and the occurrence of years with warm conditions

The effects of years with warmer than normal lake-bottom conditions on talik initiation were examined using numerical simulations over a period of 50 years, based on mean daily temperatures recorded 16 m from shore at Site 2 in 2009-11 (Table 6).

The simulations did not initiate a talik within 50 years of submergence if lake-bottom conditions were defined only with temperatures recorded in 2009-10 ($T_{lb} = 1.9^{\circ}\text{C}$, $FDD_{lb}/TDD_{lb} = 0.51 \approx \lambda_t/\lambda_f$). Talik initiation occurred during the second year after submergence when the warmer lake-bottom conditions recorded in 2010-11 ($T_{lb} = 3.3^{\circ}\text{C}$, $FDD_{lb}/TDD_{lb} = 0.18 < \lambda_t/\lambda_f$) were used as boundary conditions (Fig. 7). When warmer lake-bottom conditions were inserted every second or third year, a talik appeared three or four years after submergence, but fully refroze at least once before persisting and expand-

ing steadily. Subsequently, the freezing front moved a few cm upward into the bottom of the talik during the colder years (Fig. 7).

4.2.2. Permafrost degradation rates and FDD_{lb}/TDD_{lb}

The sensitivity of talik development rates beneath shallow water to variation in FDD_{lb}/TDD_{lb} was examined using numerical simulations over 100 years with thermal regimes that had $T_{lb} = 2.00^{\circ}\text{C}$ and FDD_{lb}/TDD_{lb} varying from 0.01 to 0.45 (Fig. 3). Simulations with mean daily temperatures were compared to a simulation based on mean annual temperature.

Time to talik initiation decreased and rates of permafrost degradation increased as FDD_{lb}/TDD_{lb} approached zero (Fig. 8). Conversely, as the ratio increased, time to talik initiation and permafrost degradation rates both became increasingly sensitive to change in FDD_{lb}/TDD_{lb} . For ratios of 0.40 to 0.43, time to talik initiation increased by 14 years, and talik depth 50 years after submergence was reduced by 24%. No talik developed during the 100 year simulation when FDD_{lb}/TDD_{lb} was ≥ 0.45 . With a constant annual mean temperature ($T_{lb} = 2.0^{\circ}\text{C}$), a numerical simulation gave similar results to thaw penetration rates with a FDD_{lb}/TDD_{lb} below 0.2 (Fig. 8).

4.2.3. Talik refreezing with $T_{lb} > 0^{\circ}\text{C}$

The third numerical simulation assessed whether talik refreezing could occur under thermal conditions observed in OCF by applying mean daily temperatures recorded at sites 2 and 3 in 2009-10 and at Site 4 in 2010-11 as boundary conditions for 100 years after a 6.5-m deep talik had been simulated. These thermal regimes had T_{lb} values ranging from 1.4 to 2.4°C and FDD_{lb}/TDD_{lb} values ranging from 0.37 to 0.65. λ_t/λ_f , which defines the

limit of permafrost sustainability if the effects of the unfrozen water content are ignored, was 0.51.

Talik refreezing did not occur when temperature regimes with $FDD_{lb}/TDD_{lb} < 0.51$, such as recorded at Site 2 in 2009-10 or at Site 4 in 2010-11 (Table 6), were applied as upper boundary conditions (Fig. 9). The talik also continued to deepen when a temperature regime with $FDD_{lb}/TDD_{lb} = 0.51$, such recorded at Site 2b (Table 6), was applied. Complete refreezing of the 6.6 m talik occurred within 50 years when temperature regimes with FDD_{lb}/TDD_{lb} of 0.60 and 0.65, recorded at sites 2a or 3b in 2009-10 (Table 6), were applied. However, when the mean daily lake-bottom temperatures for the thermal regime with $FDD_{lb}/TDD_{lb} = 0.65$, recorded at Site 3b, were replaced with the annual mean temperature, 1.4°C ($FDD_{lb}/TDD_{lb}=0$), the talik deepened.

5. Discussion

The aim of this research was to use field observations in tundra lakes of OCF and numerical simulations to investigate aspects of the lake-bottom thermal regime that control talik development near thermokarst lake shores and beneath shallow water. In the following discussion we: (1) characterize the lake-bottom thermal regime associated with $T_{lb} > 0^{\circ}\text{C}$ where water froze to the bottom and compare conditions in lakes of OCF to other areas with available information; (2) discuss controls on talik initiation beneath very shallow water near receding shores; (3) examine talik geometry and refreezing where T_{lb} is greater than but close to 0°C ; and (4) consider problems associated with the use of solutions based on T_{lb} in lakes including shallow near-shore zones.

5.1. Lake-bottom temperatures beneath shallow water

T_{lb} is used as a key variable to predict talik extent near thermokarst lakeshores. In OCF we have measured T_{lb} under a range of water depths at various distances from shore. These T_{lb} were higher than reported values from tundra lakes near the western Arctic coast, which range from -1 to -6°C in shallow areas and from 2 to 5°C where ice does not reach lake-bottom sediments [Brewer, 1958; Burn, 2002, 2005; Arp *et al.*, 2011, 2016]. At the sites examined in this paper, all T_{lb} were above 0°C (Table 6), which is similar to conditions in subarctic thermokarst lakes of central Yukon [Burn, 2003]. In central Yukon, however, ice did not reach the lake bottom and T_{lb} were higher beneath shallow water near shore than near the deeper lake centre. This is contrary to conditions observed in OCF, where frost penetrated the lake-bottom sediment near shore and T_{lb} were lower beneath shallow than deep water, similar to tundra lakes of the western Arctic.

During summer, near-shore lake-bottom temperatures in the tundra of OCF increased earlier and reached higher values than those recorded in tundra lakes of the outer Mackenzie Delta area [Burn, 2005], likely because OCF summers are warmer than near the coast and the OCF lakes are shallow. Lake-bottom temperatures in OCF did not decrease as rapidly once ice reached the sediment and remained higher than in the outer Mackenzie Delta area through the winter. This is likely due to latent and sensible heat from the talik, as winter air temperatures at Old Crow are similar to or lower than those at Tuktoyaktuk.

5.2. Talik initiation beneath shallow water

In the Mackenzie Delta region, Mackay [1992] and others observed taliks under water depths greater than approximately two-thirds of the maximum ice thickness. Following these observations it has commonly been assumed that T_{lb} is < 0°C and permafrost is

sustained beneath parts of thermokarst lakes where water freezes to the bottom early in winter [e.g., *Plug and West, 2009; Rowland et al., 2011; Matell et al., 2013*].

In this study, however, talik initiation near shore was observed under water depths less than 40% of the maximum measured ice thickness on all the transects and was sometimes found beneath water as shallow as 20 cm, or 13% of the maximum ice thickness. The presence of taliks within 10 m of receding shorelines suggests not only that permafrost was not sustainable beneath the shallow near-shore water, but also that lake-bottom conditions led to talik initiation within six years of submergence (Table 7).

Observations of talik initiation beneath such shallow water show that guidelines developed for thermokarst lakes in the outer Mackenzie Delta area, and used in other parts of the western Arctic, do not apply in OCF. These results indicate that guidelines developed in well-studied locations may not be applicable to areas where limited field data on lake-bottom temperatures and talik development are available. Further studies of talik initiation patterns beneath shallow tundra lakes and ponds should be conducted in regions representing a range of conditions to enhance our understanding of permafrost degradation beneath shallow water.

5.2.1. Necessary conditions for talik development

Near-shore talik development under shallow water in OCF appears consistent with the warm near-shore lake-bottom conditions, but the relation between T_{lb} and permafrost sustainability is moderated by λ_t/λ_f through the thermal offset [*Kudryavtsev, 1981; Burn and Smith, 1988; Romanovsky and Osterkamp, 1995*]. In our study, λ_t/λ_f was estimated to be 0.51 from two sets of lake-bottom core samples extracted at Site 1 (Table 4). Field measurements of FDD_{lb}/TDD_{lb} varied from year to year and were often close to this

value (Table 6). Hence, in OCF, the presence of taliks near shore beneath very shallow water is explained by the large TDD at the lake bottom during warm summers which balanced the FDD and difference in thermal conductivity. In the Mackenzie Delta, the “two-thirds of the maximum ice thickness” guideline uses the relation between lake depth and local maximum ice thickness as an index representing the FDD required at the lake bottom to compensate for thawing season conditions. This “two-thirds” guideline is robust where summer climatic conditions are moderated by proximity to the Arctic Ocean, such as Richards Island [Burn, 2002] and the Beaufort Coastal Plain [Arp *et al.*, 2016]. OCF, however, is an interior basin separated from the influence of the Arctic Ocean by mountains and has warmer summer conditions. As a result, the number of FDD required to balance TDD at the lake bottom is greater, and would be represented by a much smaller ratio of lake depth to maximum lake ice thickness.

Under the conditions observed in OCF, with $T_{lb} > 0^{\circ}\text{C}$ and $FDD/TDD \approx \lambda_t/\lambda_f$, small variations in FDD_{lb}/TDD_{lb} can result in important differences in talik development rate. Such variations may also determine whether or not a talik will initiate (Fig. 8) and whether or not refreezing of a talik may occur after talik initiation has begun (Fig. 9). These results support climate-change sensitivity analyses conducted for lakes with littoral shelves on Richards Island indicating that an increase in thaw-season lake-bottom temperatures and on-ice snow thickness may cause near-shore permafrost to degrade [Burn, 2002].

5.2.2. Timing of talik initiation after submergence

Simulations based on conditions recorded at our study site with $FDD_{lb}/TDD_{lb} = 0.51$ ($\approx \lambda_t/\lambda_f$) indicated that such lake-bottom thermal conditions support the continued growth of an existing talik but do not allow for the prompt talik initiation observed in the

near-shore zone at our study site (Fig. 7) (Table 7). This simulation indicated that near-shore talik initiation would not occur within 50 years of submergence unless data from 2010-11, a year with warmer lake-bottom conditions, were inserted at regular intervals in the temperature series (Fig. 7). This is consistent with *Romanovsky and Osterkamp [2000]*'s observation that the increase in unfrozen water content associated with warming of the permafrost profile following a step change in surface conditions can act as a heat sink and delay permafrost degradation after a step change in surface temperature. While the presence of taliks beneath very shallow water in OCF is partly explained by the large TDD_b during the warm summers, such taliks would not initiate close to receding shores without the intermittent occurrence of lake-bottom conditions that accelerate permafrost warming and thus facilitate the progressive increase in unfrozen water content along the permafrost profile. This emphasizes the impact of occasional years with warmer than normal lake-bottom conditions on rates of permafrost degradation where conditions are marginal for talik development. These results are of particular significance due to the amplification of northern hemisphere temperature anomalies in the Arctic, which may further facilitate talik initiation where permafrost sustainability is affected by warming conditions.

5.3. Talik geometry near receding shores in shallow lakes

Where thermal conditions result in permafrost degradation, the talik-permafrost boundary is controlled by the rate of permafrost degradation and time since submergence. If thermal conditions at the lake bottom and rates of shore recession are approximately constant, near shore talik geometry follows an exponential curve as described by the Stefan solution [*Burn and Smith, 1990*]. In the tundra lakes of OCF, where T_b was greater

than but close to 0°C, small variations in lake-bottom thermal regime could affect rates of talik expansion or result in refreezing (Fig. 8, 9). Redistribution of snow by wind on the ice surface resulted in variations in FDD_{lb}/TDD_{lb} at the lake bottom, and thus disrupted talik geometry over distances varying from 20 to 60 meters from shore (Fig. 6). Irregularities in the talik-permafrost boundary ended where water depth was > 1 m.

At Site 4, a location with relatively slow shore erosion and where water froze to the bottom over an extended area, there was a depression in the talik boundary beneath a snow drift and reduced talik depths further from the shore where the snow cover was thin. While measured T_{lb} differed by only 0.2°C at the two monitored points along the lake bottom, FDD_{lb}/TDD_{lb} varied from 0.37 to 0.44 (Table 6). Modelling showed that such changes in FDD_{lb}/TDD_{lb} , even without changes to the annual mean temperature, may cause noticeable differences in the rate of talik development, particularly for lake-bottom thermal regimes with FDD_{lb}/TDD_{lb} over 0.3 (Fig. 8). Such a difference in rate of thaw penetration would explain a talik geometry like that of Site 4 if the shoreline was static. However where the shore has been receding constantly, as at Site 4, such a geometry results from refreezing of the talik further from shore. Simulation showed that refreezing may occur when $FDD_{lb}/TDD_{lb} \geq 0.60$ (Fig. 9), and such high FDD_{lb}/TDD_{lb} were recorded at sites 2 and 3. Talik refreezing may take place despite T_{lb} values above 0°C where ice reaches the lake bottom at the sites, causing irregularities in near-shore talik geometry. This result indicates that changes in on-ice snow cover can affect permafrost sustainability beneath shallow water and emphasizes the importance of the thermal offset and interannual variability to assessments of talik development under marginal conditions.

5.4. Temporal resolution and the modelling of talik development beneath shallow water

Areas covered by shallow water that freezes to bottom are rarely taken into account when modelling talik development [e.g. *Burn, 2002; Ling and Zhang, 2003*] as they are generally assumed to have $T_{lb} \leq 0^{\circ}\text{C}$ and to sustain permafrost. Our results indicate that taliks can develop beneath very shallow water that freezes through in early winter.

The general practice when modelling talik development is to use a temporal resolution of one year for lake-bottom thermal conditions [*West and Plug, 2008; Kokelj et al., 2009; Matell et al., 2013*] so that long periods can be modelled efficiently. A finer temporal resolution is rarely used [*Zhou and Huang, 2004*]. However, talik development beneath shallow water is sensitive to aspects of lake-bottom thermal regime which may not be captured by T_{lb} and our results emphasize the importance of FDD_{lb}/TDD_{lb} to model talik development under such conditions, as FDD_{lb}/TDD_{lb} can vary widely for a given T_{lb} and affect rates of permafrost degradation (Fig. 3 and 8). In the tundra of OCF, an estimation of talik volume that excludes parts of the lakes that freeze to bottom would underestimate permafrost degradation by omitting near shore talik volume and neglecting progress in talik development prior to subsidence of the lake bottom reaching the maximum ice thickness. Finally, we note that preventing permafrost degradation is a significant component of successful design for infrastructure in the polar regions. Our results suggest that adjustments to FDD/TDD at the ground surface, perhaps by management of snow cover, may prevent or mitigate talik development near such structures.

6. Conclusions

Shallow ponds and lakes are prominent features in Arctic landscapes and their abundance is increasing due to widespread thermokarst initiation. Thermokarst lakes can be a significant source of atmospheric methane, particularly if a talik develops beneath them wherein bacteria can decompose organic matter in an anaerobic environment, year-round. Methane release from expanding taliks is particularly active at the thaw front, where organic matter formerly preserved in permafrost becomes available for decomposition. In this paper, we contribute to the understanding of permafrost degradation beneath shallow water by examining permafrost conditions near the edge of expanding thermokarst lakes in a tundra area of Old Crow Flats, northern Yukon. We used a numerical model to examine controls on talik development near thermokarst shores and beneath shallow water.

Our main findings are that:

1. Annual mean lake-bottom temperature beneath shallow water that froze to the lake bottom in early winter was above 0°C , due to high summer temperatures and on-ice near shore snow drifts during winter;
2. Taliks were found under water depths of as little as 20 cm, considerably less than $2/3$ of the maximum winter ice thickness;
3. Where ice reached the lake-bottom sediment, talik development rates were moderated by the ratio of freezing degree days to thawing degree days and the thermal offset;
4. Where annual mean temperature at the lake bottom close to shore was relatively unaffected by spatial variations in on-ice snow depth, freezing degree-days at the lake

bottom could vary sufficiently to affect rates of talik development and talik geometry beneath the lake;

5. Due to the thermal offset, variations in the ratio of freezing degree days to thawing degree days at the lake bottom may result in permafrost aggradation if the annual mean lake-bottom temperature is near but above 0°C ;

6. Where thermal conditions are marginal for talik development, interannual variations in lake-bottom thermal regime may facilitate prompt talik initiation near receding shores.

Our results emphasize that permafrost vulnerability in the near-shore zone of thermokarst lakes may be affected by regional variations in air temperature, snow fall and redistribution by wind, lake-bottom sediment, and lake bathymetry. This variability must be considered when predicting talik initiation and permafrost degradation in thermokarst landscapes. Further work may include extensive examinations of permafrost sustainability near shore and beneath the center of shallow Arctic lakes in areas with varied climatic conditions, with particular attention to the increasing frequency of warm years in circumpolar regions and to the effects of fluctuations in water levels resulting from changes in lake hydrological regimes.

7. Notation

C_a Apparent volumetric heat capacity of frozen soil, including latent heat effects ($\text{J m}^{-3} \text{ }^{\circ}\text{C}^{-1}$).

$C_{i,w,o,m}$ Volumetric heat capacity of ice, water, organic material, mineral soil ($\text{J m}^{-3} \text{ }^{\circ}\text{C}^{-1}$).

$C_{f,t}$ Volumetric heat capacity of frozen and unfrozen soil ($\text{J m}^{-3} \text{ }^{\circ}\text{C}^{-1}$).

FDD, TDD Freezing degree days, thawing degree days.

V_i Volumetric excess ice content (%).

L Latent heat required to thaw the water contained in a given volume of soil (kJ m^{-3}).

n Number of items considered.

V_o Volumetric content of organic material ($\text{m}^3 \text{ m}^{-3}$).

p Porosity ($\text{m}^3 \text{ m}^{-3}$).

Q Applied boundary heat flux (W m^{-1}).

t Time (s).

t_{tr} Time between submergence and the end of seasonal frost penetration in the lake bottom (s).

T Temperature ($^{\circ}\text{C}$).

$T_{g,ps,lb}$ Annual mean temperature measured at the depth of zero annual amplitude, near the permafrost surface, on the lake bottom ($^{\circ}\text{C}$).

$u\%$ Proportion of soil pore water that is unfrozen ($\text{m}^3 \text{ m}^{-3}$).

$V_{ss,sw}$ In a thawed core sample: volume of saturated sediment, volume of supernatant water (cm^3).

w_u Gravimetric unfrozen water content (g g^{-1}).

z Depth below the ground surface (m).

θ, θ_u Volumetric total water content, and unfrozen water content ($\text{m}^3 \text{ m}^{-3}$).

$\lambda_{f,t}$ Thermal conductivity of frozen ground and thawed ground ($\text{J s}^{-1} \text{ m}^{-1} \text{ }^{\circ}\text{C}^{-1}$).

$\lambda_{i,w,o,m}$ Thermal conductivity of ice, water, organic material, mineral soil ($\text{J s}^{-1} \text{ m}^{-1} \text{ }^{\circ}\text{C}^{-1}$).

$\lambda_{x,y}$ Horizontal and vertical thermal conductivity of the ground ($\text{J s}^{-1} \text{ m}^{-1} \text{ }^{\circ}\text{C}^{-1}$).

Acknowledgments. The research was supported by the Government of Canada International Polar Year program, the National Science and Engineering Research Council of Canada, the Polar Continental Shelf Program, Natural Resources Canada, and the Northern Scientific Training Program, Indigenous Affairs and Northern Development Canada. Essential logistical support was provided by the Vuntut Gwitchin First Nation Government and the Aurora Research Institute, Inuvik. Several field technicians contributed to data collection including A.L. Frost, B. Brown, D. Charlie, K. Tetlich, L. Nagwan, M. Frost Jr., S. Njoutli, S. Frost, and C.Z. Braul. The lake-bottom temperature, bathymetry, talik depth, and on-ice snow depth data used in this analysis are available on Figshare (doi:10.6084/m9.figshare.3119578). We thank S.W. Gruber, S.A. Wolfe, B.M. Jones, S.V. Kokelj, and several anonymous referees for helpful comments which improved the paper.

References

- Andersland, O. B., and B. Ladanyi (2003), *Frozen Ground Engineering, 2nd edn*, John Wiley and Sons, Hoboken.
- Arp, C. D., B. M. Jones, F. E. Urban, and G. Grosse (2011), Hydrogeomorphic processes of thermokarst lakes with grounded-ice and floating-ice regimes on the Arctic Coastal Plain, Alaska, *Hydrological Processes*, 25(15), 2422–2438, doi:10.1002/hyp.8019.
- Arp, C. D., B. M. Jones, G. Grosse, A. C. Bondurant, V. E. Romanovsky, K. M. Hinkel, and A. D. Parsekian (2016), Threshold sensitivity of shallow Arctic lakes and sublake permafrost to changing winter climate, *Geophysical Research Letters*, doi:10.1002/2016GL068506.

Bintanja, R., and F. M. Selten (2014), Future increases in Arctic precipitation linked to local evaporation and sea-ice retreat, *Nature*, 509(7501), 479–482, doi:10.1038/nature13259.

Blackwell, D., and M. Richards (2004), Geothermal map of North America, *map, 1 sheet, scale: 1:6,500,00*, American Association of Petroleum Geologists, Tulsa.

Brewer, M. C. (1958), The thermal regime of an Arctic lake, *Transactions, American Geophysical Union*, 39(2), 278, doi:10.1029/TR039i002p00278.

Burn, C. R. (1997), Cryostratigraphy, paleogeography, and climate change during the early Holocene warm interval, western Arctic coast, Canada, *Canadian Journal of Earth Sciences*, 34(7), 912–925, doi:10.1139/e17-076.

Burn, C. R. (2002), Tundra lakes and permafrost, Richards Island, western Arctic coast, Canada, *Canadian Journal of Earth Sciences*, 39(8), 1281–1298, doi:10.1139/e02-035.

Burn, C. R. (2003), Lake-bottom thermal regime in thermokarst terrain near Mayo, Yukon Territory, Canada, in *Proceedings of the Eighth International Conference on Permafrost, Zurich, Switzerland, July 21 25, 2003*, edited by M. Phillips, L. Arenson, and S. Springman, pp. 113–118, Balkema Publishers, Lisse.

Burn, C. R. (2005), Lake-bottom thermal regimes, western Arctic coast, Canada, *Permafrost and Periglacial Processes*, 16(4), 355–367, doi:10.1002/ppp.542.

Burn, C. R., and C. A. S. Smith (1988), Observations of the “thermal offset” in near-surface mean annual ground temperatures at several sites near Mayo, Yukon Territory, Canada, *Arctic*, 41, 99–104.

Burn, C. R., and M. W. Smith (1990), Development of thermokarst lakes during the Holocene at sites near Mayo, Yukon Territory, *Permafrost and Periglacial Processes*,

1(2), 161–175, doi:10.1002/ppp.3430010207.

Duguay, C. R., and P. M. Lafleur (2003), Determining depth and ice thickness of shallow sub-Arctic lakes using space-borne optical and SAR data, *International Journal of Remote Sensing*, 24(3), 475–489, doi:10.1080/01431160304992.

Duk-Rodkin, A., R. W. Barendregt, D. G. Froese, F. Weber, R. Enkin, I. Rod Smith, G. D. Zazula, P. Waters, and R. Klassen (2004), Timing and extent of Plio-Pleistocene glaciations in north-western Canada and east-central Alaska, in *Developments in Quaternary Sciences, Glaciations-Extent and Chronology Part II: North America*, vol. 2, Part B, edited by J. Ehlers and P.L. Gibbard, pp. 313–345, Elsevier, Amsterdam.

EBA Engineering Consultants Ltd (1982), Old Crow groundwater supply: A geotechnical, hydrological and thermal study, *Report to Yukon Territorial Government*, EBA Engineering Consultants Ltd, Whitehorse.

GEO–SLOPE International Ltd (2010), *Thermal modeling with TEMP/W 2007: an engineering methodology, Fourth Edition*, GEO-SLOPE International, Ltd., Calgary.

Gray, D. R., and B. T. Alt (2001), *Resource description and analysis of Vuntut National Park of Canada*, Parks Canada, Whitehorse.

Hwang, C., and M. W. Smith (1973), Thermal disturbance due to channel shifting, Mackenzie delta, NWT, Canada, in *Proceedings of the Second International Conference on Permafrost, Yakutsk, USSR, 13-28 July, 1973, North American Contribution*, vol. 2, edited by F. Sanger and P. Hyde, p. 51, National Academy of Sciences, Washington DC.

Johansen, O. (1975), Thermal Conductivity of Soils,, Ph.D. Thesis, Institutt for Kjøleteknikk, Trondheim, (CRREL Draft Translation 637, 1977).

Kennedy, K., and D. G. Froese (2008), Aggregate resource exploration using a process-depositional model of meltwater channel development in the Eagle Plains area, northern Yukon, in *Yukon Exploration and Geology 2007*, edited by D. Emond, L. Blackburn, R. Hill, and L. Weston, pp. 169–178, Yukon Geological Survey, Whitehorse.

Kessler, M. A., L. J. Plug, and K. M. Walter Anthony (2012), Simulating the decadal-to millennial-scale dynamics of morphology and sequestered carbon mobilization of two thermokarst lakes in NW Alaska, *Journal of Geophysical Research: Biogeosciences*, *117*(G2), G00M06, doi:10.1029/2011JG001796.

Kokelj, S. V., and C. R. Burn (2003), Ground ice and soluble cations in near-surface permafrost, Inuvik, Northwest Territories, Canada, *Permafrost and Periglacial Processes*, *14*(3), 275–289, doi:10.1002/ppp.458.

Kokelj, S. V., T. C. Lantz, J. Kanigan, S. L. Smith, and R. Coutts (2009), Origin and polycyclic behaviour of tundra thaw slumps, Mackenzie Delta region, Northwest Territories, Canada, *Permafrost and Periglacial Processes*, *20*(2), 173–184, doi:10.1002/ppp.642.

Kokelj, S. V., T. C. Lantz, S. A. Wolfe, J. C. Kanigan, P. D. Morse, R. Coutts, N. Molina-Giraldo, and C. R. Burn (2014), Distribution and activity of ice wedges across the forest-tundra transition, western Arctic Canada, *Journal of Geophysical Research: Earth Surface*, *119*(9), 2032–2047, doi:10.1002/2014JF003085.

Kudryavtsev, V. (Ed.) (1981), *The Permafrost Study (in Russian)*, Moscow University Press, Moscow.

Lachenbruch, A. H., M. C. Brewer, G. W. Greene, and B. Vaughn Marshall (1962), Temperatures in permafrost, in *Temperature; Its Measurement and Control in Science and Industry, Volume 3. Part 1: Basic Concepts, Standards and Methods*, vol. 3, edited

by C. Herzfeld and F. Brickwedde, p. 791, Reinhold Publishing Corp., London.

Lantz, T. C., and K. W. Turner (2015), Changes in lake area in response to thermokarst processes and climate in Old Crow Flats, Yukon, *Journal of Geophysical Research: Biogeosciences*, 120(3), 513–524, doi:10.1002/2014JG002744.

Lauriol, B., Y. Cabana, J. Cinq-Mars, M.-A. Geurts, and F. W. Grimm (2002), Cliff-top eolian deposits and associated molluscan assemblages as indicators of late Pleistocene and Holocene environments in Beringia, *Quaternary International*, 87(1), 59–79, doi:10.1016/S1040-6182(01)00062-3.

Lauriol, B., D. Lacelle, S. Labrecque, C. R. Duguay, and A. Telka (2009), Holocene evolution of lakes in the Bluefish Basin, northern Yukon, Canada, *Arctic*, 62(2), 212–224, doi:10.14430/Arctic133.

Lichti-Federovich, S. (1973), Palynology of six sections of Late Quaternary sediments from the Old Crow River, Yukon Territory, *Canadian Journal of Botany*, 51(3), 553–564, doi:10.1139/b73-066.

Ling, F., and T. Zhang (2003), Numerical simulation of permafrost thermal regime and talik development under shallow thaw lakes on the Alaskan Arctic Coastal Plain, *Journal of Geophysical Research: Atmospheres*, 108(D16), 4511, doi:10.1029/2002JD003014.

Mackay, J. R. (1963), The Mackenzie Delta area, NWT, *Geographical Branch, Memoir 8*, Department of Mines and Technical Surveys, Ottawa.

Mackay, J. R. (1992), Lake stability in an ice-rich permafrost environment: examples from the western Arctic coast., in *Aquatic Ecosystems in Semi-arid Regions: Implications for Resource Management, August 27-30, 1990, Saskatoon, Canada*, edited by R. Robarts and M. Bothwell, no. 7 in N.H.R.I. Symposium Series, pp. 1–25, National Hydrology

Research Institute, Environment Canada, Saskatoon.

Maloney, E. D., S. J. Camargo, E. Chang, B. Colle, R. Fu, K. L. Geil, Q. Hu, X. Jiang, N. Johnson, K. B. Karnauskas, J. Kinter, B. Kirtman, S. Kumar, B. Langenbrunner, K. Lombardo, L. N. Long, A. Mariotti, J. E. Meyerson, K. C. Mo, J. D. Neelin, Z. Pan, R. Seager, Y. Serra, A. Seth, J. Sheffield, J. Stroeve, J. Thibeault, S.-P. Xie, C. Wang, B. Wyman, and M. Zhao (2013), North American climate in CMIP5 experiments: Part III: assessment of twenty-first-century projections, *Journal of Climate*, *27*(6), 2230–2270, doi:10.1175/JCLI-D-13-00273.1.

Matell, N., R. S. Anderson, I. Overeem, C. Wobus, F. E. Urban, and G. D. Clow (2013), Modeling the subsurface thermal impact of Arctic thaw lakes in a warming climate, *Computers and Geosciences*, *53*, 69–79, doi:10.1016/j.cageo.2011.08.028.

Matthews, J. V. J., C. E. Schweger, and J. A. Janssens (1990), The last (Koy-Yukon) interglaciation in the northern Yukon: evidence from Unit 4 at Ch'ijee's Bluff, Bluefish Basin, *Géographie physique et Quaternaire*, *44*(3), 341–362, doi:10.7202/032835ar.

Morgenstern, A., G. Grosse, F. Günther, I. Fedorova, and L. Schirrmeister (2011), Spatial analyses of thermokarst lakes and basins in Yedoma landscapes of the Lena Delta, *The Cryosphere*, *5*(4), 849–867, doi:10.5194/tc-5-849-2011.

Olefeldt, D., S. Goswami, G. Grosse, D. Hayes, G. Hugelius, P. Kuhry, A. D. McGuire, V. E. Romanovsky, A. B. K. Sannel, E. a. G. Schuur, and M. R. Turetsky (2016), Circumpolar distribution and carbon storage of thermokarst landscapes, *Nature Communications*, *7*, 13,043, doi:10.1038/ncomms13043.

Ovenden, L. (1985), Hydroseral histories of the Old Crow peatlands, northern Yukon, Ph.D. thesis, University of Toronto, Toronto.

Plug, L. J., and J. J. West (2009), Thaw lake expansion in a two-dimensional coupled model of heat transfer, thaw subsidence, and mass movement, *Journal of Geophysical Research: Earth Surface*, 114(F1), F01,002, doi:10.1029/2006JF000740.

Rampton, V. N. (1988), Quaternary geology of the Tuktoyaktuk Coastlands, Northwest Territories, *Memoir 423*, Geological Survey of Canada, Ottawa.

Riseborough, D. W. (2002), The mean annual temperature at the top of permafrost, the TTOP model, and the effect of unfrozen water, *Permafrost and Periglacial Processes*, 13(2), 137–143, doi:10.1002/ppp.418.

Romanovsky, V. E., and T. E. Osterkamp (1995), Interannual variations of the thermal regime of the active layer and near-surface permafrost in northern Alaska, *Permafrost and Periglacial Processes*, 6(4), 313–335.

Romanovsky, V. E., and T. E. Osterkamp (2000), Effects of unfrozen water on heat and mass transport processes in the active layer and permafrost, *Permafrost and Periglacial Processes*, 11(3), 219–239, doi:10.1002/1099-1530(200007/09)11:3<219::AID-PPP352>3.0.CO;2-7.

Rowland, J. C., B. J. Travis, and C. J. Wilson (2011), The role of advective heat transport in talik development beneath lakes and ponds in discontinuous permafrost, *Geophysical Research Letters*, 38(17), L17,504, doi:10.1029/2011GL048497.

Roy-Leveillee, P., and C. R. Burn (2015), Geometry of oriented lakes in Old Crow Flats, northern Yukon, in *Proceedings of the Sixty-eighth Canadian Geotechnical Conference and Seventh Canadian Permafrost Conference, Quebec City, Canada, September 20-23, 2015*, Canadian Geotechnical Society, Richmond, paper 284.

Roy-Leveillee, P., and C. R. Burn (2016), A modified landform development model for the topography of drained thermokarst lake basins in fine-grained sediments, *Earth Surface Processes and Landforms*, 41(11), 1504–1520, doi:10.1002/esp.3918.

Roy-Léveillé, P., C. R. Burn, and I. D. McDonald (2014), Vegetation-permafrost relations within the forest-tundra ecotone near Old Crow, northern Yukon, Canada, *Permafrost and Periglacial Processes*, 25(2), 127–135, doi:10.1002/ppp.1805.

Schwamborn, G. J., J. K. Dix, J. M. Bull, and V. Rachold (2002), High-resolution seismic and ground penetrating radargeophysical profiling of a thermokarst lake in the western Lena Delta, Northern Siberia, *Permafrost and Periglacial Processes*, 13(4), 259–269, doi:10.1002/ppp.430.

Sheldrick, B. H. (1984), Analytical methods manual. Research Branch, *LRRI contribution no. 84-30*, Research Branch, Agriculture Canada, Ottawa.

Smith, M. W., and D. W. Riseborough (1996), Permafrost monitoring and detection of climate change, *Permafrost and Periglacial Processes*, 7(4), 301–309.

Smith, M. W., and D. W. Riseborough (2002), Climate and the limits of permafrost: a zonal analysis, *Permafrost and Periglacial Processes*, 13(1), 1–15, doi:10.1002/ppp.410.

Smith, M. W., and A. R. Tice (1988), Measurement of the unfrozen water content of soils: Comparison of NMR and TDR methods, *CRREL report 88-18*, US Army Corps of Engineers, Cold Regions Research and Engineering Laboratory, Hanover.

Stevens, C. W., B. J. Moorman, and S. M. Solomon (2010), Modeling ground thermal conditions and the limit of permafrost within the nearshore zone of the Mackenzie Delta, Canada, *Journal of Geophysical Research*, 115(F4), doi:10.1029/2010JF001786.

Taylor, A., S. Dallimore, and J. Wright (2008), Thermal impact of Holocene lakes on a permafrost landscape, Mackenzie Delta, Canada, in *Proceedings of the 9th International Conference on Permafrost, Fairbanks, Alaska, 29 June-3 July 2008, Vol. 2*, edited by D. Kane and K. M. Hinkel, pp. 1757–1762, Institute for Northern Engineering, University of Alaska Fairbanks, Fairbanks.

Walter, K. M., S. A. Zimov, J. P. Chanton, D. Verbyla, and F. S. Chapin (2006), Methane bubbling from Siberian thaw lakes as a positive feedback to climate warming, *Nature*, 443(7107), 71–75, doi:10.1038/nature05040.

West, J. J., and L. J. Plug (2008), Time-dependent morphology of thaw lakes and taliks in deep and shallow ground ice, *Journal of Geophysical Research: Earth Surface*, 113(F1), F01,009, doi:10.1029/2006JF000696.

Williams, P. J., and M. W. Smith (1989), *The Frozen Earth: Fundamentals of Geocryology*, Cambridge University Press, Cambridge.

Yukon Ecoregions Working Group (2004), *Ecoregions of the Yukon Territory: Biophysical Properties of Yukon Landscapes*, no. 04-01 in PARC Technical Bulletin, Agriculture & Agri-Food Canada, Summerland.

Zazula, G. D., A. Duk-Rodkin, C. E. Schweger, and R. E. Morlan (2004), Late Pleistocene chronology of Glacial Lake Old Crow and the north-west margin of the Laurentide ice sheet, in *Quaternary Glaciations-Extent and Chronology Part II: North America, Developments in Quaternary Sciences*, vol. 2B, edited by J. Ehlers and P.L. Gibbard, pp. 347–362, Elsevier, London.

Zhou, W., and S. Huang (2004), Modeling impacts of thaw lakes to ground thermal regime in northern Alaska, *Journal of Cold Regions Engineering*, 18(2), 70–87, doi:

10.1061/(ASCE)0887-381X(2004)18:2(70).

Accepted Article

Table 1. Annual Mean Air Temperature (AMAT), Freezing Degree Days (FDD) and Precipitation at Old Crow from September 1st to August 31st, 2008-11^a

	2008-09	2009-10	2010-11
AMAT (°C)	-9.4	-6.5	-8.3
<i>FDD</i> (°C d)	4813	4016	4540
<i>FDD</i> (°C d) before Dec. 1	1016	942	766
Total precipitation (mm)	352	344	721

^a Environment Canada data are available at <http://climate.weather.gc.ca/>, accessed on January 16th, 2014

Table 2. Lakeshore Morphology, Vegetation Cover, and Water Depth 40 m from Shore at the four Study Sites.

Site	Aspect, fetch (m)	Bank height (m) ^a	Bank slope (°) ^{ab}	Water depth (m)	Bank slope vegetation	Bank top vegetation
1	NE, 4000	3.0	35-90	2.2	Exposed soil	Low shrub tundra
2	NE, 1600	1.0	35	2.3	Exposed soil	Low shrub tundra
3	NW, 1200	2.6	35	1.4	Tall shrubs	Tall shrub tundra
4	SW, 1600	2.0	30	0.4	Tall shrubs	Tall shrub tundra

^a The shore bank is above water, hence bank slope and height are subaerial.

^b The bank slope near Site 1 varied during each open-water season depending on rates of thermo-denudation and sediment removal by wave erosion.

Table 3. Boundary Conditions and Ground Properties used for Numerical Simulations of Talik Development

Condition or Property ^a	Value
Porosity (m ³ m ⁻³)	0.49
Vol. excess ice (%)	0
Vol. latent heat (kJ m ⁻³)	1.5 x 10 ⁵
Thawed vol. heat capacity (kJ m ⁻³ °C ⁻¹)	3270
Frozen vol. heat capacity (kJ m ⁻³ °C ⁻¹)	2170
Thawed thermal conductivity (W m ⁻¹ °C ⁻¹)	1.12
Frozen thermal conductivity (W m ⁻¹ °C ⁻¹)	2.20
Geothermal heat flow (W m ⁻¹)	0.07

^a Ground properties estimated from samples of permafrost collected at Site 1.

Table 4. Porosity, Excess Ice, and Organic Matter Content in Samples from two Lake-Bottom Permafrost Cores Extracted Near a Rapidly Receding Shoreline^a

Depth below top of bank (m)	Depth below top of bore hole (m)		Vol. moisture content (%)		Vol. excess-ice content (%)		Grav. organic content (%)	
	A	B	A	B	A	B	A	B
3.3 - 3.5	0.8 - 1.0	0.9 - 1.1	45	54	0	0	10	6
3.5 - 3.7	1.0 - 1.2	1.1 - 1.3	60		9	0		6
3.7 - 3.9	1.2 - 1.4	1.3 - 1.5	51	58	0	0	7	3
3.9 - 4.1	1.4 - 1.6		54		0	0		8
4.1 - 4.3	1.6 - 1.8		39		0	0		6
4.3 - 4.5	1.8 - 2.0		50		0	0		4
4.5 - 4.7	2.0 - 2.2		40		0	0		5

^a The cores were collected in collected in May 2010. The height of the adjacent shore bank was 2.5 m. Material between 2.5 and 3.3 m beneath the top of the bank was not sampled to avoid fallen material.

Table 5. Annual Mean Temperature near the Top of Permafrost (T_{ps} ; °C) and Mean Snow Depth (m) at Sites 2 to 4^a

Site	T_{ps} (°C)	Snow depth (m)	T_{ps} (°C)	Snow depth (m)	T_{ps} (°C)
	2008-09	March 2009	2009-10	March 2010	2010-11
2	-5.4	0.34	-4.8	0.37	-4.0
3	-3.3	0.77	-3.5	0.44	-3.2
4	-4.4	0.75	-4.0	0.37	-3.5

^a Snow depth was measured at the temperature sensors. No temperature sensor was installed at Site 1 due to rapid shore erosion, but surface conditions were similar to Site 2.

Table 6. Snow Depth, Date of Contact (Month/Day) Between Ice and Sediment, Ratio of Freezing to Thawing Degree

Days (FDD_{tb}/TDD_{tb}), and Annual Mean Lake-Bottom Temperature (T_{tb}) at the Sites^{a,b}

Site	Distance from shore (m)	Water depth (m)	2008-2009			2009-2010			2010-2011			
			Snow depth (m)	Contact date	$\frac{FDD_{tb}}{TDD_{tb}}$	T_{tb} (°C)	Snow depth (m)	Contact date	$\frac{FDD_{tb}}{TDD_{tb}}$	T_{tb} (°C)	Contact date	$\frac{FDD_{tb}}{TDD_{tb}}$
1 ^b	12	1.8	0.27	03/04	0.01	4.0	0.17	03/13	0.00	4.5	0.00	4.9
2a	6	0.7	0.45	10/05	0.53	1.4	0.20	10/28	0.60	1.5	10/19	0.58
2b	16	1.1	0.17	11/13	0.51	1.5	0.11	11/21	0.51	1.9	12/15	0.18
3a	12	0.7	0.70	10/19	0.54	1.4	0.19	11/03	0.64	1.4	10/16	0.56
3b	20	1.1	0.20	11/13	0.59	1.3	0.09	11/16	0.65	1.4	10/17	0.18
4a	15	0.4					1.35				10/04	0.37
4b	35	0.6					0.12				10/31	0.44

^a Snow depth on lake ice was measured at the end of March in 2009 and 2010.

^b The temperature sensor associated with Site 1 was located 400 m to the NW of the transect where the bank was more stable, the snow drift shallower, and the water deeper than where the transect used for bathymetry and talk depth measurements was located (Fig. 1b).

Table 7. Distance from the Shoreline to the Edge of the Talik and Conditions Associated with Talik Initiation^a

Site	Distance to Talik (m)	Water depth (m)	Max. snow depth (m)	Frost penetration depth ^b (m)	Time before talik initiation (yr)
1	6(±1)	0.5	>2.2	0.5 (±0.1)	1.3 (±0.2)
2	10 (±1)	0.6	0.7	1.1 (±0.1)	5.0 (±0.2)
3	2 (±1)	0.4	1.2	0.3 (±0.1)	5.7 (±0.4)
4	0	0.2	2.3	0.4 (±0.1)	

^a Frost penetration below the lake bottom was measured near shore, where the talik begins. Time before talik initiation was calculated based on erosion rates measured between 2009 and 2011 (Table 8).

^b Depth of frost penetration in the lake bottom was measured in spring 2009 at sites 1, 3, and 4, and in spring 2010 at Site 2. The values reported in the table were measured at the edge of the talik.

Table 8. Rates of Shoreline Erosion at Each Study Site^a

Site	1951-1996 (m yr ⁻¹)	Spring 2009 to autumn 2011 (m yr ⁻¹)
1	2.00 (±0.07)	3.9 (±0.1)
2	0.92 (±0.04)	1.8 (±0.4)
3	0.33 (±0.04)	0.7 (±0.2)
4	0.13 (±0.06)	0.0 (±0.3)

^a Erosion rates for 1951-1996 were obtained from aerial photographs and rates for 2009-2011 were based on field measurements. Erosion at Site 4 was only monitored over the 2010 and 2011 open water seasons.

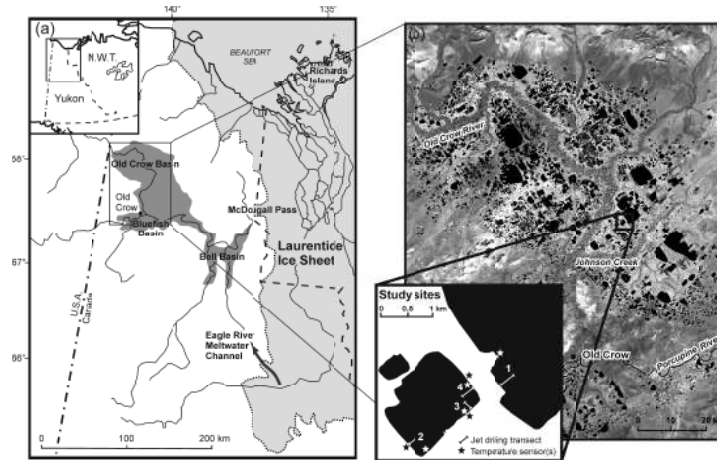


Figure 1. (a) Northern Yukon with extent of Glacial Lake Old Crow in the Bell, Bluefish, and Old Crow basins. The approximate maximum limit of the Laurentide Ice Sheet is shown in light grey (after *Rampton, 1988, Fig. 55; Zazula et al., 2004, Fig. 1; Kennedy and Froese, 2008, Fig. 2, Lauriol et al., 2009, Fig. 1*). (b) Landsat 7 orthoimage of Old Crow Flats and surrounding areas acquired on August 30th 2001 (©Department of Natural Resources Canada. All rights reserved). Waterbodies are in black, and the locations of the study sites are indicated on the inset.

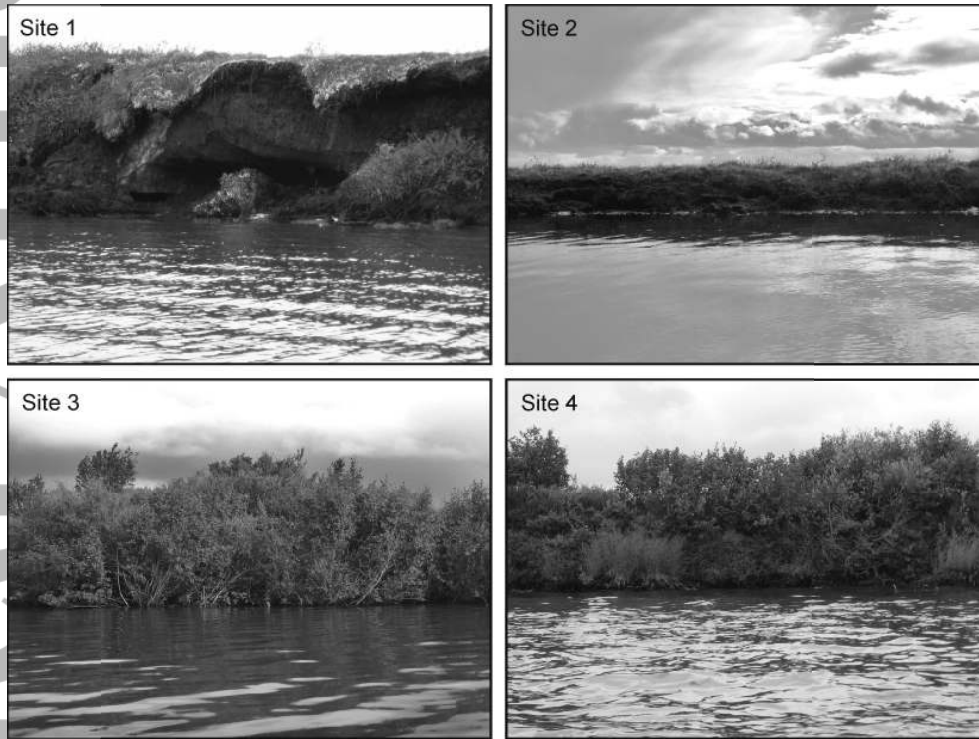


Figure 2. The four shorelines from which transects were extended over lake ice to measure snow depth, lake depth, lake-bottom temperature, and talik depth. Bank heights for sites 1 to 4 were 3.0 m, 1.0 m, 2.6 m, and 2.0 m, respectively.

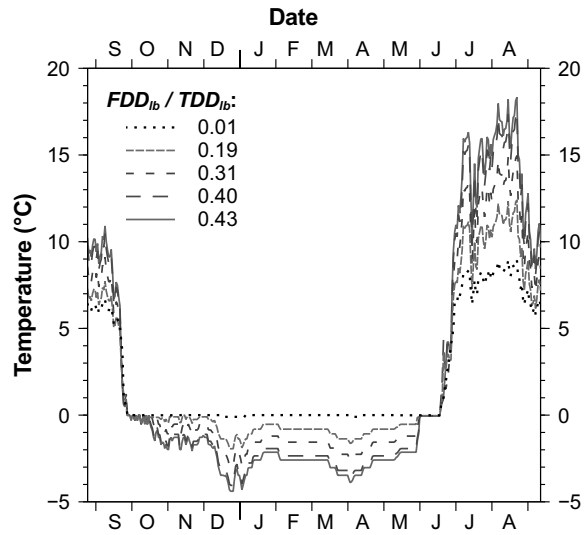


Figure 3. Six simulated thermal regimes of varying amplitude with $T_{lb} = 2.00^{\circ}\text{C}$ and 252 days of ice contact with the lake bottom used for the numerical examination of talik development sensitivity to variations in FDD_{lb}/TDD_{lb} .

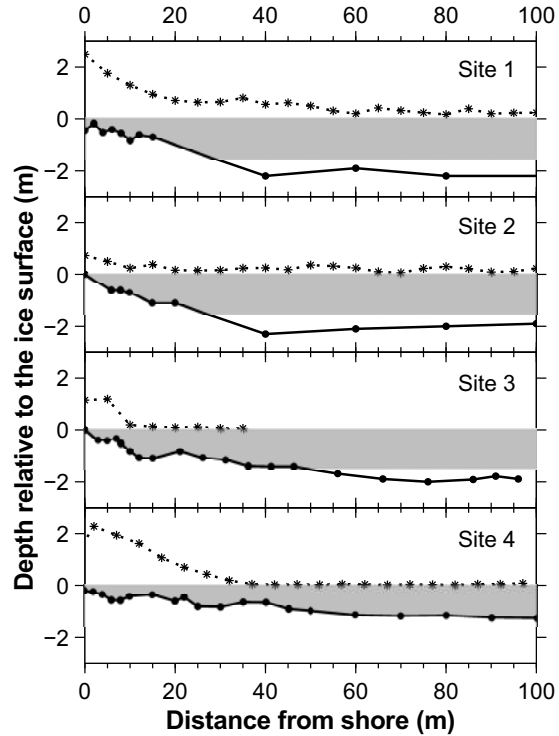


Figure 4. Near-shore bathymetry and snow depth at the four sites. The dotted line represents the snow thickness on the ice surface, with asterisks marking measurement points, and the grey area represents the average local maximum ice thickness, both based on measurements in March 2010. The solid line is the lake bottom, with black circles marking measurement points.

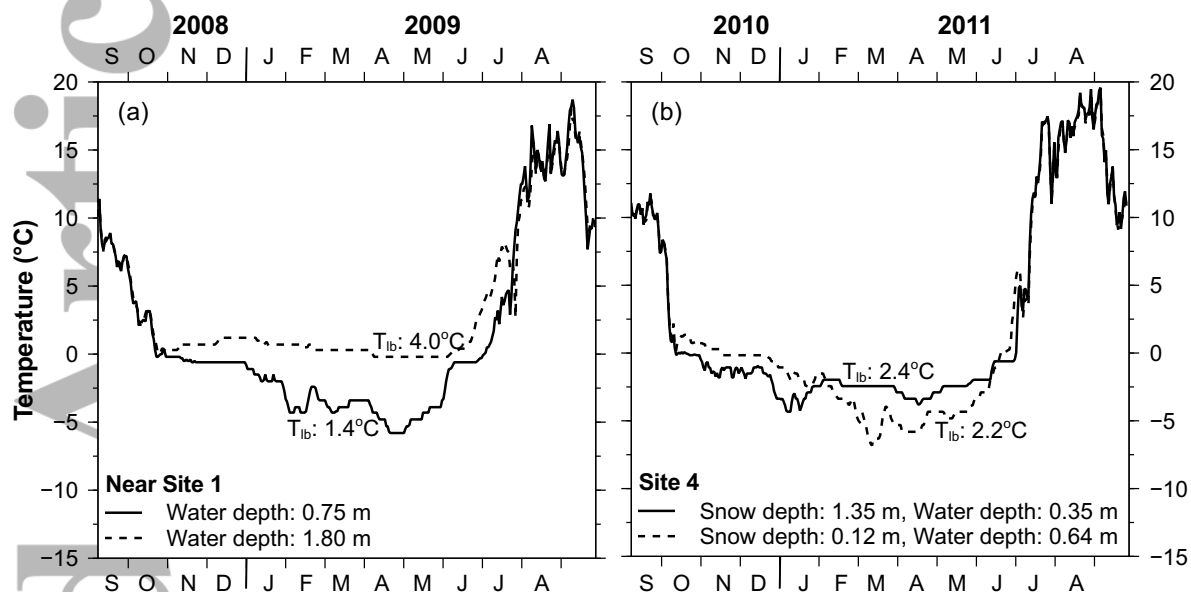


Figure 5. Effects of water and snow depths on lake-bottom temperatures. (a) Thermal regimes NE and SW of Site 1 (Fig.1b), where ice reached the lake bottom at 75 cm depth and where water depth (180 cm) was greater than lake-ice thickness. The annual mean lake-bottom temperatures at these sites were 1.4°C and 4.0 °C respectively. (b) Thermal regimes 12 and 20 m from shore at Site 4, where frost penetrated lake-bottom sediments but snow depth, controlled by the drift at the lake shore, modified the effects of water depth. The annual mean lake-bottom temperatures beneath and outside the snow drift were 2.4°C and 2.2°C respectively.

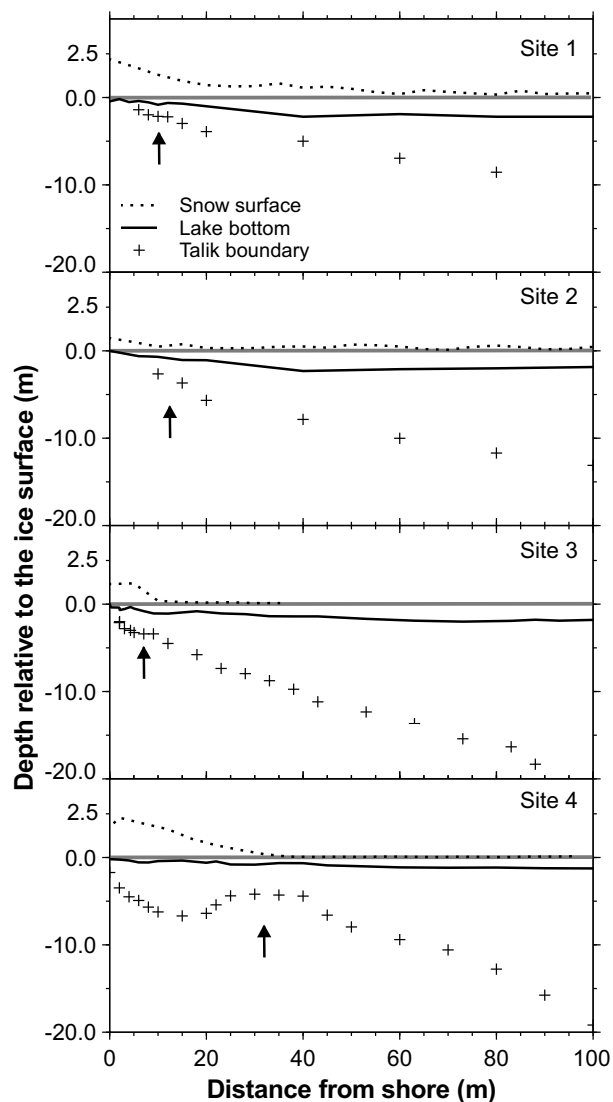


Figure 6. Near-shore talik depth relative to the ice surface (elevation = 0, marked with a solid line) measured by jet drilling along each transect. Snow depth was measured in March 2010 and talik depths were measured in May and early June of 2009 and 2010. The near-shore irregularity (small shelf) in the talik basal slope is indicated with an arrow in each graph. Note the difference in y-axis scale above and below the ice surface, resulting in a vertical exaggeration of 2 for snow thickness relative to lake and talik depths.

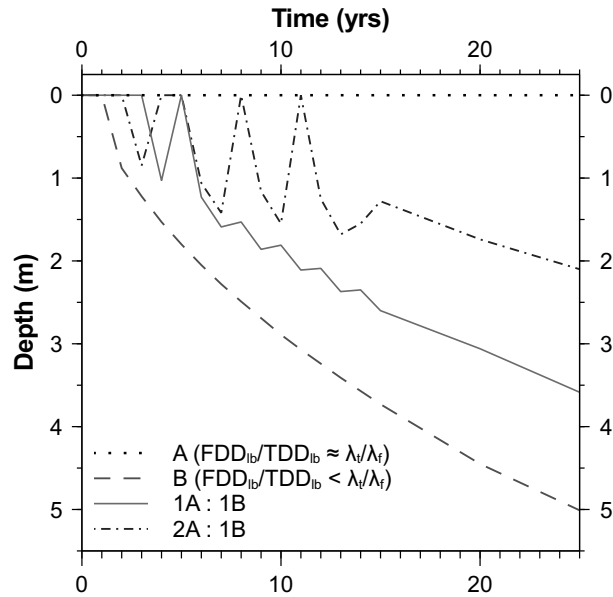


Figure 7. The first 25 years of a 50-year simulation of talik initiation and development after submergence with daily mean lake-bottom temperatures measured at Site 2 in 2009-10 (A) where $T_{lb} = 1.9^{\circ}\text{C}$ and $FDD_{lb}/TDD_{lb} = 0.51 \approx \lambda_t/\lambda_f$, and 2010-11 (B), a year with warmer than usual lake-bottom conditions with $T_{lb} = 3.3^{\circ}\text{C}$ and $FDD_{lb}/TDD_{lb} = 0.18$. Temperature data from 2009-10 and 2010-11 were alternated (1A:1B), or data from 2010-11 were inserted one year out of three (2A:1B). No talik developed under A.

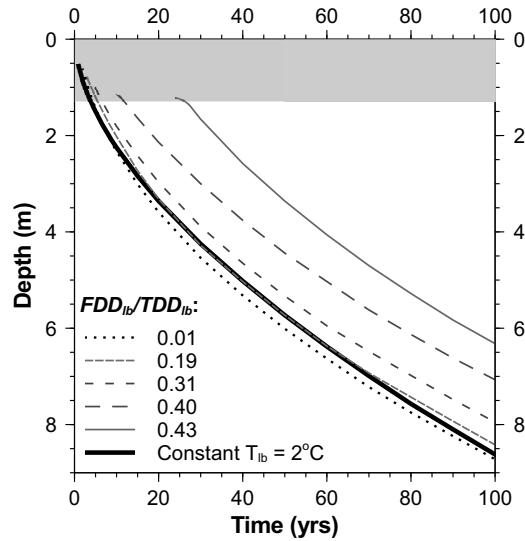


Figure 8. Talik development rates associated with six simulated thermal regimes of varying amplitude with $T_{lb} = 2.00^{\circ}\text{C}$ and 252 days of ice contact with the lake bottom (Fig. 3). Talik depth was defined as the maximum depth of ground that remained below 0°C year round. Thermal regimes with $FDD_{lb}/TDD_{lb} \geq 0.45$ did not lead to the development of a talik within 100 years and are not shown. The maximum active-layer depth simulated with the thermal regimes shown was 1.28 m, with $FDD_{lb}/TDD_{lb} = 0.43$, and is indicated with grey shading in the upper portion of the graph.

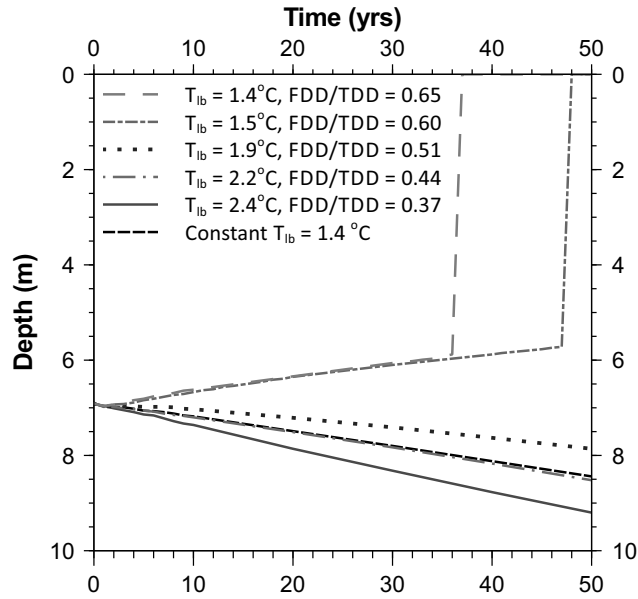


Figure 9. Talik development and refreezing with six different lake-bottom thermal regimes applied after a talik has developed to a depth of 6.5 m. The lines represent the 0°C for each of the six simulations. From top to bottom in the legend, the data used were collected at sites 3b, 2a, 2b, in 2009-10 and at sites 4b, 4a in 2010-11 (Table 6). A constant lake-bottom temperature of 1.4°C was applied at the lake bottom for $T_{lb} = 1.4^{\circ}\text{C}$.